

Mesoscopic interparticle potentials in the lattice Boltzmann equation for multiphase fluids

R. S. Qin

CCLRC Daresbury Laboratory, Warrington WA4 4AD, United Kingdom

(Received 6 December 2005; published 7 June 2006)

I introduce a method to derive mesoscopic particle interactions by macroscopic thermodynamics, which is suitable for simulation of multiphase fluids by means of the lattice Boltzmann equation. For van der Waals fluids, the interaction possesses a high-density strong repulsive core and a low-density weak attractive tail, which looks like the Lennard-Jones potential with replacement of the distance between particles with mass density. Numerical results on phase separation show a droplet growth scheme rather than spinodal decomposition, and exhibit accurately the equilibrium phase diagram, a convincing interfacial energy property, and irreversible thermodynamics.

DOI: [10.1103/PhysRevE.73.066703](https://doi.org/10.1103/PhysRevE.73.066703)

PACS number(s): 47.11.-j, 02.70.Ns, 05.70.Ce

Particle methods compute the system evolution according to given interparticle potentials, such as the Lennard-Jones potential in molecular dynamics and the soft repulsive pairwise potential in dissipative particle dynamics [1]. The lattice Boltzmann (LB) equation, although particles are only allowed to move from one lattice to another without falling in between, is a particle-based computational technique that involves interactions and collisions [2]. Shan and Chen first studied the mesoscale interparticle potentials [3]. After a decade of development, LB methods have achieved a state of sophistication and have shown considerable success in the simulation of flows and phase transitions of a wide variety of mesoscopic fluids under various constraints, such as wetting and jamming at interfaces [4,5]. However, irreversible thermodynamics has been the weak point of the LB model. A few LB models overcome the difficulty by either introducing new equilibrium particle distribution functions (called equilibria hereafter) that compromise the free energy contribution, e.g., the free energy model [4], or adding an artificial body force that creates the irreversible effect [6]. He and Doolen pointed out recently that an interparticle potential with short-range strong Enskog repulsive and long-range weak mean field attractive interactions can produce LB kinetic theory that is consistent with thermodynamics [7]. The aim of the present work is to introduce a generic method to derive the mesoscopic interactions from the macroscopic thermodynamics without referring to microscopic or artificial parameters, and to examine the equilibrium thermodynamic properties and nonequilibrium transport phenomena of the LB system with the derived potentials. We begin by considering the LB equation with a Bhatnagar-Gross-Krook collision term,

$$f_i(\vec{r} + \hat{e}_i \Delta t, t + \Delta t) - f_i(\vec{r}, t) = -\frac{1}{\tau} [f_i(\vec{r}, t) - f_i^{eq}(\vec{r}, t)] \quad (1)$$

where $f_i(\vec{r}, t)$ is the distribution function moving with speed \hat{e}_i at lattice point \vec{r} and time t . τ is the collision time which is related to the kinetic viscosity of the fluid. $f_i^{eq}(\vec{r}, t)$ represents the equilibria. \hat{e}_i and $f_i^{eq}(\vec{r}, t)$ depend on the lattice model and their values have been derived previously [8]. For the lattice with N non-zero discrete speed vectors, $\rho(\vec{r}, t) = \sum_{i=0}^N f_i(\vec{r}, t)$ is the mass density and $\vec{u}(\vec{r}, t) = \sum_{i=0}^N f_i(\vec{r}, t) \hat{e}_i / \rho(\vec{r}, t)$ the speed of

the lattice when the particle interactions are completely neglected. Following the Shan-Chen model [3], one defines the interaction potential between lattice points \vec{r} and \vec{r}' as

$$V(\vec{r}, \vec{r}') = \varphi w(\vec{r}, \vec{r}') \psi(\vec{r}) \psi(\vec{r}') \quad (2)$$

where φ is a signal function that will be specified later in the paper. $w(\vec{r}, \vec{r}')$ is the weight factor that depends on the relative position between r and r' . $\psi(\vec{r})$ is a function of macroscopic quantities at lattice point \vec{r} , e.g., the mass density and solute compositions. The interparticle potential presented in Eq. (2) is based on phenomenological assumptions and possesses no microscopic mechanism to ensure the validity of the irreversible thermodynamics. The second law of thermodynamics is ensured by proper definition of $\psi(\vec{r})$. In the present work, $\psi(\vec{r})$ will be derived from the macroscopic thermodynamics. In the following, we confined ourselves to an isothermal and chemically homogeneous (no segregation) system and therefore $\psi(\vec{r}) = \psi(\rho(\vec{r}))$. The particle interactions cause a change of particle momentum, and give the lattice speed in the form $u(r, t) = \sum_{i=0}^N f_i(r, t) \hat{e}_i / \rho(r, t) - \tau \nabla [\sum_{r' \neq r} V(r, r')] / \rho(r, t)$. Multiplying Eq. (1) by 1 and summing over subscript i will lead to a continuum equation, and multiplying Eq. (1) by \hat{e}_i and summing over subscript i leads to the Navier-Stokes equation with the equation of state at the long-wavelength limit given by

$$p = \rho RT + \frac{\varphi RT}{2} \psi(\rho)^2, \quad (3)$$

which should be identical to the equation of state derived from thermodynamics.

The total free energy for an isothermal and chemically homogeneous system is taken to be

$$G = \int \left(\frac{\varepsilon}{2} |\nabla \rho(\vec{r})|^2 + g[\rho(\vec{r}), T] \right) dr \quad (4)$$

where ε is the gradient parameter, and $g[\rho(\vec{r}), T]$ is the free energy density of the bulk phase with mass density $\rho(\vec{r})$ and temperature T . The equation of state is [4]

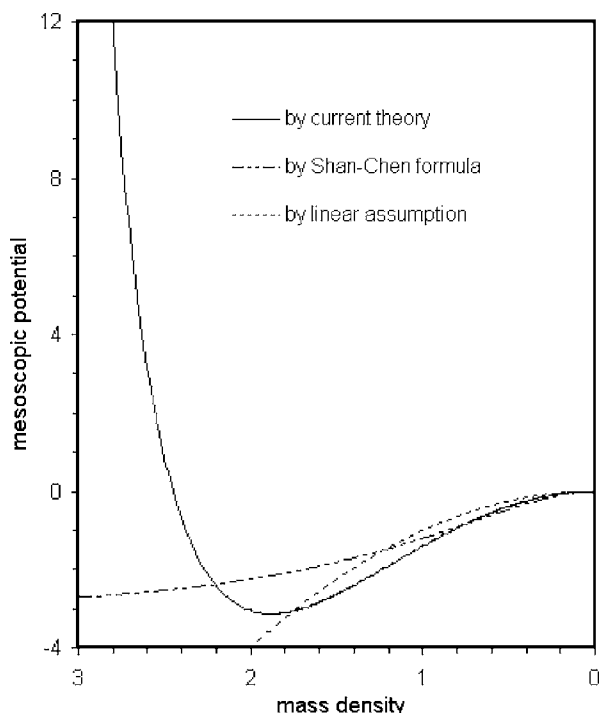


FIG. 1. Mesoscopic interparticle potentials for van der Waals fluid by the present theory with parameters of $\eta=0$, $a=1.018\,226$, $b=0.3$, and $T=0.9$ (solid line), Shan-Chen model of $\psi(\rho)=\rho_0[1-\exp(\rho/\rho_0)]$ with $\rho_0=1$ and $\varphi=3$ (dashed and dotted lines), and linear assumption of $\psi(\rho)=\rho$. The unit of the mesoscopic potential is Joules when the unit of the mass density is kg/m^3 .

$$p = \rho \frac{\partial g[\rho, T]}{\partial \rho} - g[\rho, T]. \quad (5)$$

Equations (3) and (5) should be identical. One has

$$\frac{1}{2} \varphi \psi(\rho)^2 = \left(\rho \frac{\partial g[\rho, T]}{\partial \rho} - g[\rho, T] \right) / RT - \rho. \quad (6)$$

φ has been naturally defined by Eq. (6): $\varphi=-1$ when the right-hand side of Eq. (6) is negative, or $\varphi=1$ when it is positive. In the LB model, each lattice represents a subsystem that contains large amounts of atoms or molecules. Equation (6) is, therefore, suitable for computing interparticle potentials on each lattice which is a subsystem and obeys statistical mechanics. To reflect the statistical fluctuation, one adds a noise term to $\psi(\rho(\vec{r}))$:

$$\psi(\rho(\vec{r}, t)) = \psi \left(\sum_{i=0}^N f_i(\vec{r}, t) + \eta \xi \right), \quad (7)$$

where $|\eta| \ll 1$ is the noise intensity and ξ is a random function between -1 and 1 . The form of the statistical fluctuation has been widely applied in phase-field models for computing the kinetic driving force in the simulation of solidification [9].

I have now built up the relationship between the mesoscopic interaction parameter $\psi(\rho(\vec{r}))$ and the free energy density $g[\rho(\vec{r}), T]$. To prove the validity of the method I have carried out a case study for van der Waals fluids. The free

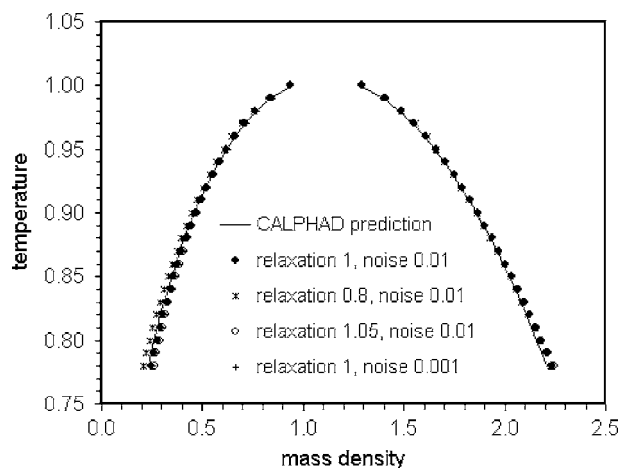


FIG. 2. Mass density at equilibrium by numerical simulations (scattered symbols) and by theoretical calculation of equilibrium phase diagram (solid line). The temperature is the reduced temperature (with respect to the reference temperature).

energy density of the bulk fluid is taken to be

$$g[\rho(\vec{r}), T] = \rho RT \ln \left(\frac{\rho}{1 - \rho b} \right) - a \rho^2 \quad (8)$$

where a and b are constant parameters for given materials. One chooses the energy unit as RT_f in which T_f is the reference temperature. T is the reduced temperature relative to T_f . The mesoscopic interparticle potential in the long-wavelength limit, $\varphi \psi(\rho)^2$, is calculated by Eqs. (6)–(8) and plotted in Fig. 1 for $\eta=0$, $a=1.018\,226$, $b=0.3$, and $T=0.9$. The interaction potential is repulsive when $\rho \geq 2.45$ and the strength increases sharply with growth of the mass density. In the region of $0 < \rho < 2.45$, a weak attractive interparticle force exists. The overall shape of the interaction potential is similar to the Lennard-Jones potential which is widely used

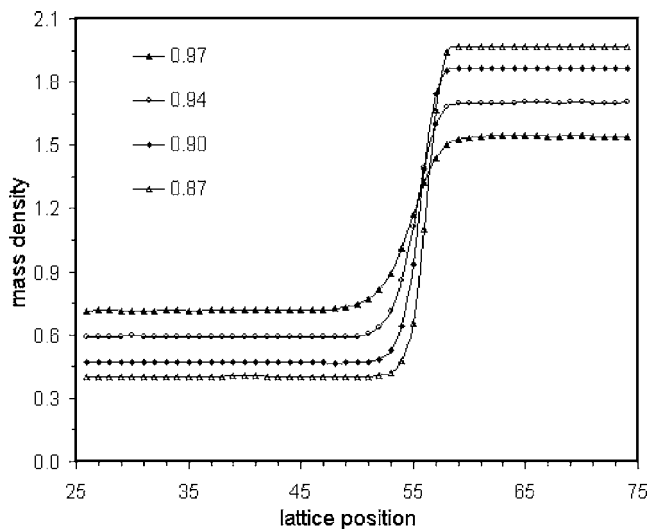


FIG. 3. Equilibrium density profiles normal to a planar interface for a van der Waals fluids for temperatures 0.87, 0.9, 0.94, and 0.97, respectively. The unit of the mass density is the same as in Fig. 1.

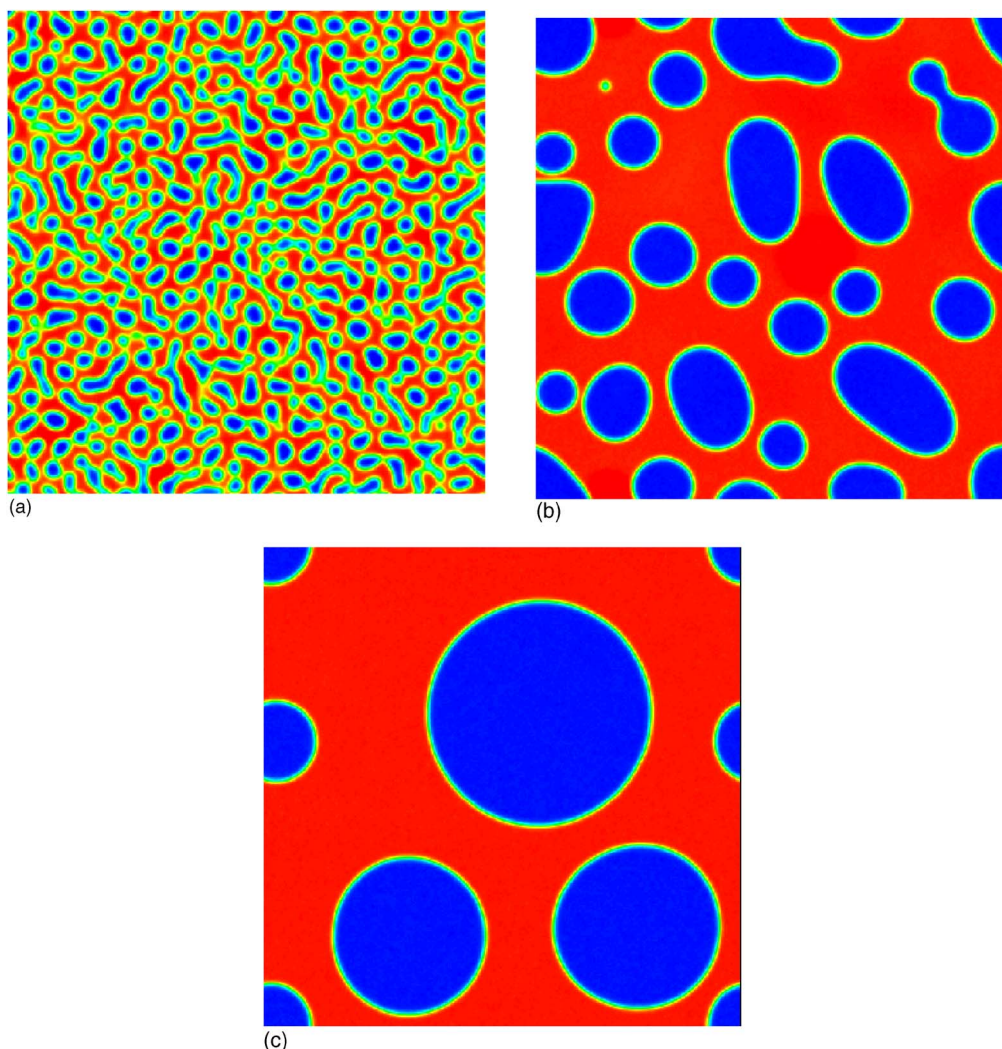


FIG. 4. (Color online) Time evolution of phase separation. $t =$ (a) 375, (b) 3750, and (c) 34 120. The simulations were performed on a 512×512 lattice at $T=0.98$.

in molecular dynamics simulations. The strong repulsive force plays the role of the hard core. The interaction approaches zero when $\rho \rightarrow 0$, which creates the ideal gas limitation. The mesoscopic potential suggested by Shan and Chen, with $\psi(\rho) = \rho_0[1 - \exp(\rho/\rho_0)]$, is also plotted in Fig. 1 with $\rho_0=1$ and $\phi=3$. The interparticle potential in the Shan-Chen formula is a monotonic function of mass density and approaches a finite value for large mass density, which can produce phase separation, but sometimes the patterns easily lost. The linear assumption of $\psi(\rho) = \rho$, which has been commented on Ref. [7], is also plotted in Fig. 1. The linear assumption inevitably leads to mass collapse because the larger mass density possesses larger attraction. The geometric shape of the mesoscopic interparticle potential developed in the current work is similar to the microscopic description by He and Doolen [7]. Its equilibrium and nonequilibrium thermodynamic properties will be examined in the following.

Numerical simulations are performed in a D2Q9 (two-dimensional and nine-speed lattice Boltzmann model) 100×100 lattice space with the same values of a and b mentioned earlier in the paper. One chooses noise intensity η

$=0.01$, initial mass density $\rho=1.2$ and particles distributed uniformly, relaxation time $\tau=1$, homogeneous temperature distribution with initial value of $T=1$ but dropping by 0.01 after each 10 000 time steps, $f_i^{eq} = \rho w_i [1 + 3(\hat{e}_i \cdot \vec{u}) + 4.5(\hat{e}_i \cdot \vec{u})^2 - 1.5\vec{u}^2]$, $w_0=4/9$, and $w_i=1/9$ for $i=1, 2, 3, 4$ and $w_i=1/36$ for $i=5, 6, 7, 8$. The periodic boundary condition is applied. The fluid phase separates into two rectangular domains and leaves two planar interfaces (a sphere will have a smaller surface area only when the volume fraction of one of the phases is less than $1/\sqrt{\pi}$). The time steps of 10 000 are found sufficient for the system to achieve the equilibrium state. The mass densities in each bulk phase at equilibrium for different temperature are recorded and plotted in Fig. 2 as scattered symbols. On the other hand, the standard routine for calculation of a phase diagram (CALPHAD), i.e., the common tangent law and minimization of the system free energy at fixed system volume and total mass, is performed and the theoretical predictions are plotted in Fig. 2 as solid lines. Numerical simulations using the mesoscopic interaction defined in the present paper are in good agreement with CALPHAD predictions, which suggests that the correct equi-

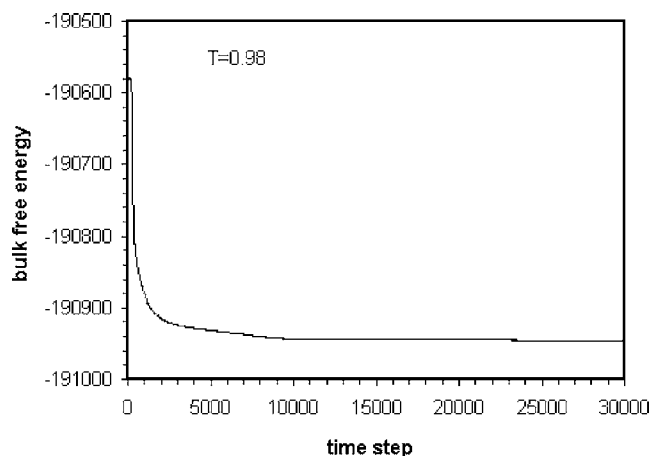


FIG. 5. Time evolution of bulk free energy during phase separation. The unit of bulk free energy is multiplied by the volume of a lattice cell.

librium thermodynamic properties are reproduced accurately. To study the effect of relaxation time and noise intensity on the phase equilibrium, one has also computed the above described system with different parameters of $\eta=0.01$ with $\tau=0.8$, $\eta=0.01$ with $\tau=1.05$, and $\eta=0.001$ with $\tau=1$, respectively. The numerical results are also presented in Fig. 2 as scattered symbols. It was found that the kinetic parameters have negligible effect on the equilibrium phase diagram. It is worth emphasizing that the mass density differences between two adjacent phases in several simulations are more than one order of magnitude. The mass density profile across the interface is, as illustrated in Fig. 3 for temperature of 0.87, 0.9, 0.94, and 0.97, in good agreement with classical interface theory.

The transient behavior of phase separation is studied in a D2Q9 512×512 lattice with $T=0.98$. Other parameters take the same values as presented in the earlier part of the work ($\eta=0.01$, $\tau=1$, and the others the same as before). Figure 4 shows the domain morphology at time steps of 375, 3750, and 34 120 separately. The initial system is uniform. The noise term that represents the statistical fluctuation in Eq. (7) causes the nucleation of new phases. Although the initial bubble nuclei are small, the mass densities inside the droplets are close to their equilibrium value, as illustrated in Fig. 4(a). The small bubbles are coalescing and form larger and larger bubbles as the time evolves. Figure 4(b) contains coalescing bubbles in the view field. Spherical bubbles are illustrated in Fig. 4(c). The interface during the system evolution is clear and of the same thickness. In the simulation, the mass density at each lattice point is calculated and their values are inserted into Eq. (8) for the calculation of the free energy of the bulk phase. The evolution of the bulk free energy is illustrated in Fig. 5. The bulk free energy is not the total system free energy because the gradient contribution has not been counted. However, the contribution from the mass gradient to the system energy decreases as the interface area is reduced due to bubble coalescence during system evolution. The bulk free energy illustrated in Fig. 5 shows that the free energy of the system is dropping during phase separation. The irreversible thermodynamics in the scheme is, therefore, obeyed.

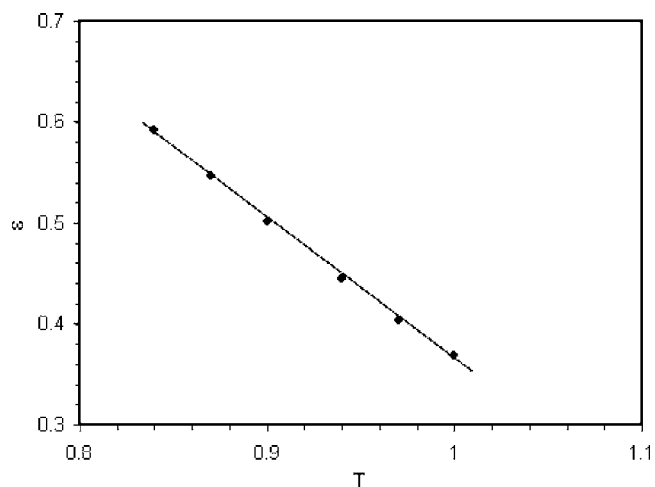


FIG. 6. Interfacial energy coefficient with respect to temperature. The scattered points are from statistical calculation by using Eq. (9). The straight line is $\varepsilon \approx 1.77 - 1.4T$. T is the reduced temperature.

The numerical stability in particle methods is related to the time step. The time step is determined by the stiffness of the particle interactions. A softer potential allows a larger time step. The interparticle potentials derived in the present work, as illustrated in Fig. 1, are substantially softer than the potentials given by a hard sphere model. The numerical simulation in the current work is found very stable and the system free energy decreases toward the equilibrium value monotonically. He *et al.* studied the numerical instability caused by the stiffness of the hard sphere model (Enskog's theoretical treatment of the exclusion-volume effect) in the LB simulation and suggested a modification scheme to reduce the effect of stiff repulsion [10]. The basic idea of the modification is to multiply by a small factor so that the original stiffness is reduced substantially. For some softer interparticle repulsions, such as the pair interaction potential that was used in dissipative particle dynamics, the numerical scheme can be stable for an even larger time step [11].

The interfacial energy has been the crucial and most difficult point to address in LB models. The thermodynamic theory requires the relationship between surface tension and gradient of density in the form [12]

$$\sigma^{heo} = \varepsilon \int_{-\infty}^{+\infty} |\nabla \rho|^2 dz \quad (9)$$

where ε is a constant for an isothermal system and $\varepsilon = \varepsilon_0 - \varepsilon_T T$ ($\varepsilon_T > 0$) when the thermocapillary effects are included [13]. However, the nearest-neighbor LB model gives the surface tension $\sigma^{LB} = (\rho/2) \int_{-\infty}^{+\infty} |\nabla \psi|^2 dz$, which implies that the nearest-neighbor-based LB models will be thermodynamically inconsistent unless $\psi(\rho) = \sqrt{\varepsilon} \rho$ [7]. In the current work one has

$$|\nabla \psi|^2 = \left[\frac{b - 0.5\rho b^2}{(1 - \rho b)^2} - \frac{a}{T} \right]^2 \bigg/ \left(\frac{b}{1 - \rho b} - \frac{a}{T} \right) |\nabla \rho|^2. \quad (10)$$

To study the discrepancy between thermodynamic theory and

our model, I calculated $\varepsilon = \Sigma_r |\nabla \psi(\rho(\vec{r}, T))|^2 / \Sigma_r |\nabla \rho|^2$ for those numerical data that Figs. 2 and 3 are also based on, and have plotted the result in Fig. 6. A linear relationship between ε and T is revealed. Data fitting shows $\varepsilon \approx 1.77 - 1.4T$, which is in good agreement with thermodynamic theory on surface tension with thermocapillary effects [13]. It implies that the discrepancy between the interface properties obtained by the current work and the thermodynamic theory is negligible.

The reason for the correct reproduction of interface properties can be understood from a combination of Fig. 3 and Eq. (9). It can be seen from Fig. 3 that the interface thickness is slightly different at different temperatures. The interface

energy is related not only to density gradient but also to the interfacial thickness, as expressed in Eq. (9). Take into account the effect of interfacial thickness as well as the density gradient gives the correct interface properties.

In summary, I have developed a method to define mesoscopic interparticle potentials according to the macroscopic free energy, which gives good agreement with equilibrium properties, such as the phase diagram and interfacial energy, and nonequilibrium behavior such as irreversible thermodynamics.

This work was supported by EPSRC under Grant No. GR/R99584.

-
- [1] J. Koplik and J. R. Banavar, *Science* **257**, 1664 (1992); R. D. Groot and R. B. Warren, *J. Chem. Phys.* **107**, 4423 (1997).
- [2] G. R. McNamara and G. Zanetti, *Phys. Rev. Lett.* **61**, 2332 (1988); Y. H. Qian, D. Dhumieres, and P. Lallemand, *Europhys. Lett.* **17**, 479 (1992); S. Chen and G. D. Doolen, *Annu. Rev. Fluid Mech.* **30**, 329 (1998).
- [3] X. W. Shan and H. D. Chen, *Phys. Rev. E* **47**, 1815 (1993).
- [4] M. R. Swift, W. R. Osborn, and J. M. Yeomans, *Phys. Rev. Lett.* **75**, 830 (1995).
- [5] K. Stratford, R. Adhikari, I. Pagonabarraga, J. C. Desplat, and M. E. Cates, *Science* **309**, 2198 (2005).
- [6] A. K. Gunstensen, D. H. Rothman, S. Zaleski, and G. Zanetti, *Phys. Rev. A* **43**, 4320 (1991).
- [7] X. Y. He and G. G. Doolen, *J. Stat. Phys.* **107**, 309 (2002).
- [8] X. Y. He and L. S. Luo, *Phys. Rev. E* **55**, R6333 (1997).
- [9] J. A. Warren and W. J. Boettinger, *Acta Metall. Mater.* **43**, 689 (1995); R. S. Qin and E. R. Wallach, *Acta Mater.* **51**, 6199 (2003).
- [10] X. Y. He, S. Y. Chen, and R. Y. Zhang, *J. Comput. Phys.* **152**, 642 (1999).
- [11] R. D. Groot, *J. Chem. Phys.* **118**, 11265 (2003).
- [12] S. M. Allen and J. W. Cahn, *Acta Metall.* **27**, 1085 (1979).
- [13] R. Borcia, D. Merkt, and M. Bestehorn, *Int. J. Bifurcation Chaos Appl. Sci. Eng.* **14**, 4105 (2004).